ISBN: 978-3-95450-233-2 ISSN: 2673-5504 doi:10.18429/JACoW-SRF2021-TUPFAV001

# PROGRESS ON SRF LINAC DEVELOPMENT FOR THE ACCELERATOR-DRIVEN SUBCRITICAL SYSTEM AT JAEA*

B. Yee-Rendon†, Y. Kondo, J. Tamura, S. Meigo and F, Maekawa, JAEA/J-PARC,Tokai-mura, Japan

*Abstract*

To overcome the nuclear waste problem, the Japan Atomic Energy Agency (JAEA) has been developing an accelerator-driven subcritical system (ADS) since the late 1980s. In the JAEA-ADS proposal, an 800 MWth subcritical reactor is driven by a 30 MW cw proton linear accelerator (linac). The biggest challenges for the ADS machines are the high reliability and availability required for their operations. To this end, the present JAEA-ADS linac was redesigned by adopting the current developments in Superconducting Radio-Frequency (SRF) technology. Additionally, we developed a robust lattice to control the beam loss and implemented a fault-tolerance scheme for the fast recovery of SRF cavity failures. This work presents the latest results of the R&D of the JAEA-ADS superconducting linac.

## INTRODUCTION

The Japan Atomic Energy Agency (JAEA) is designing an Accelerator Driven Subcritical System (ADS) to deal with nuclear waste by transmuting minor actinides. Figure 1 presents the general scheme for the JAEA-ADS. The project consists of a 30 MW cw proton accelerator, a Spallation target, and an 800 MW thermal power subcritical reactor [1]. Table 1 provides a summary of the specifications for the JAEA-ADS linac.

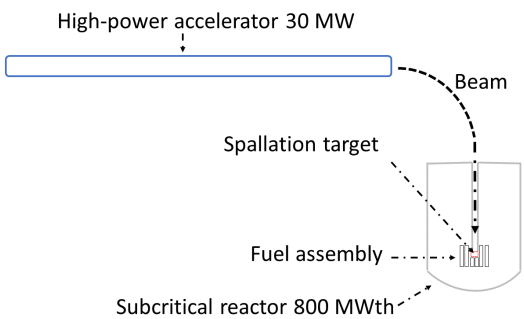


Figure 1: General scheme for the ADS.

The accelerator for the JAEA-ADS requires to operate in cw to be compatible with the reactor operation and accelerates a 20 mA proton beam up to an energy of 1.5 GeV. In addition, high reliability in the accelerator is demanded to avoid thermal stress in the subcritical reactor elements. Thus, the previous requirements indicate a Superconducting Radio-Frequency (SRF) linear accelerator (linac) is the most suitable candidate for this task. From the specifications presented in Table 1, reliability is the biggest challenge. The reliability for the ADS is higher than the achieved in the present high-intensity linacs [2, 3]; to this end, the JAEA-ADS SRF linac pursues a robust beam optics design and fault-tolerance capabilities to become a reliability-oriented accelerator [4].

Table 1: Main Characteristics of the JAEA-ADS Accelerator

| Parameter | | Beam trip duration |
|---|---|---|
| Particle | Proton | |
| Beam current (mA) | 20 | |
| Beam energy (GeV) | 1.5 | |
| Duty factor (%) | 100 (cw) | |
| Beam loss (W/m) | < 1 | |
| Beam trips per year [5] | $2\times10^4$ | ≤ 10 s |
| | $2\times10^3$ | from 10 s to 5 min |
| | 42 | > 5 min |

## BEAM OPTICS DESIGN

To achieve a robust beam optic design: the lattice must have strict control of beam loss, have a simple configuration, and operates with de-rated SRF cavities to reduce the failure probabilities. Moreover, we want to reduce the number of cavities and the linac length to minimize the operational cost.

Our linac starts with a normal conducting injector up to an energy of some MeVs, following to the state of the art of high-intensity SRF linacs [6–8]. Then, an SRF section, the so-called main linac, provides the rest of the acceleration. The main linac supplies most of the beam energy and represents the largest part of the linac length. Thus, we designed the main linac lattice to satisfies the above conditions.

To achieve an efficient design in terms of the numbers of cavities and length, we use three different types of SRF cavities: Half Wave Resonator (HWR), Single Spoke Resonator (SSR), and five-cell Elliptical Resonator (EllipR). The main linac is divided into five sections and operates with three different frequencies, as is shown in Fig 2. Table 2 presents a description of the section layouts using the following notation: C= cavity, S= solenoid, DQ= doublet quadrupole.

Table 2: Lattice Configuration in the Main Linac

| **Section** | **Layout** | **Period (m)** | **Total cavities** |
|---|---|---|---|
| HWR | S-C | 0.7 | 25 |
| SRR1 | S-$C^2$ | 1.7 | 66 |
| SSR2 | S-$C^3$ | 3.4 | 72 |
| EllipR1 | DQ-$C^3$ | 5.7 | 60 |
| EllipR2 | DQ-$C^5$ | 9.9 | 70 |

* Work supported by Subvention for ADS development.
† byee@post.j-parc.jp

ISBN: 978-3-95450-233-2 ISSN: 2673-5504 doi:10.18429/JACoW-SRF2021-TUPFAV001

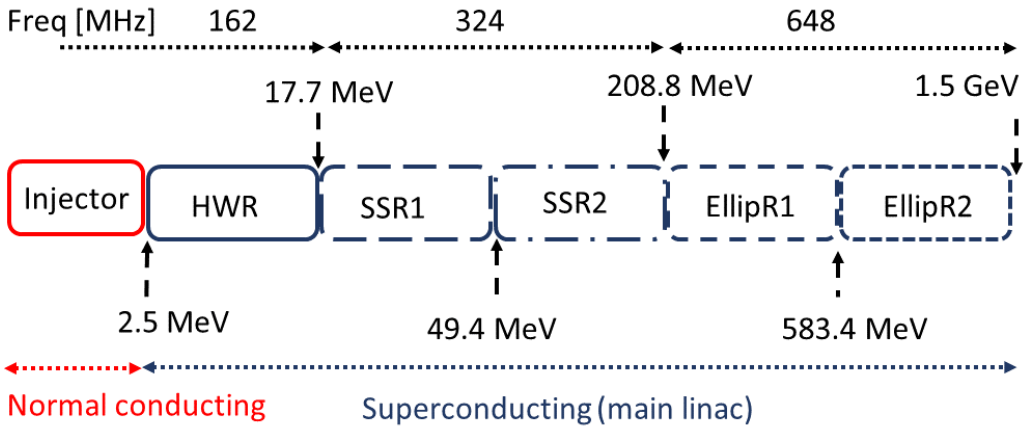


Figure 2: Linac lattice configuration.

The accelerating gradients ($E_{acc}$) of the SRF cavities are de-rated to operate with an electric peak of 30 MV/m inside the SRF element to minimize operation malfunctions. Additionally, the operation with conservative $E_{acc}$ values enables fault-tolerance compensations in case of an SRF cavity failure.

The beam optics follows an equipartitioning condition, phase advance per period ($\sigma$) lower than 90 deg, among others conditions [9, 10]. The lattice design and the beam tracking simulations were done using the TraceWin program [11]. We tested the robustness of the beam optics by tracking large beam distributions with $1x10^7$ macroparticles obtained from the RFQ design [12]. Table 3 presents the relevant parameters of the main linac.

Table 3: Parameters of the Main Linac

| **Parameters** | |
|---|---|
| Input $\varepsilon_{norm,rms,x}$ ($\pi$ mm mrad) | 0.24 |
| Input $\varepsilon_{norm,rms,y}$ ($\pi$ mm mrad) | 0.23 |
| Input $\varepsilon_{norm,rms,z}$ ($\pi$ MeV deg/mm mrad) | 0.08/0.39 |
| Number of Cavities | 293 |
| Number of magnets | 153 |
| Length (m) | 416 |

The performance test using large beam distributions shows that the linac lattice did not record any beam loss, the control of emittance growth was about 10 % on all the planes, and the beam envelopes are well contained in the linac aperture.

Figure 3 shows the evolution of the $\varepsilon_{norm,rms}$ along the linac on the three planes. The emittance growth is small on the $x$ and $z$ planes. The $y$ plane has the highest emittance growth; however, the increase was about 10 %. The transverse rms and maximum envelopes are presented in Fig. 4. The evolution of rms is smooth along the linac, and the maximum size showed some envelope increase at the transition between SSR2 and EllipR1. Nevertheless, there is enough space between the aperture and the envelopes to ensure not beam loss. Table 4 summarizes the beam optics performance of the model.

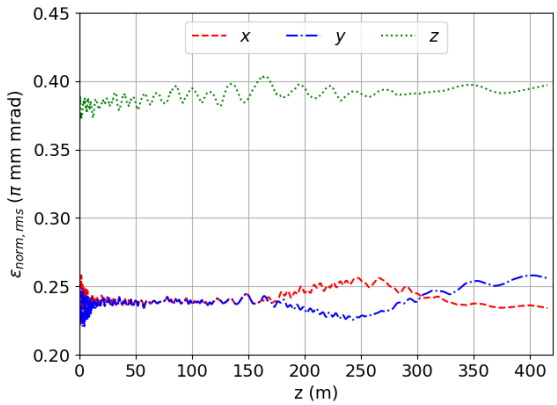


Figure 3: Normalized rms emittance in the linac.

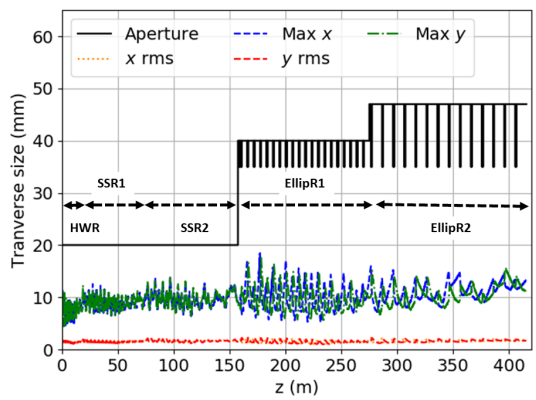


Figure 4: Maximum and rms transverse beam size along the main linac. The aperture is physical aperture of the elements that composed the main linac.

ISBN: 978-3-95450-233-2 ISSN: 2673-5504 doi:10.18429/JACoW-SRF2021-TUPFAV001



Table 4: Summary of Beam Optics Performance of the Main Linac

| **Parameters** | Value *x*/*y*/*z* |
|---|---|
| Beam power lost (W/m) | 0 |
| $\varepsilon_{norm,rms}$ growth (%) | 3.7/10.8/1.2 |
| Maximum transverse size (mm) | 13.3/11.2 |
| rms transverse size (mm) | 1.9/ 1.6 |

## FAULT-TOLERANCE

The ADS linac requires high control in the number of beam trips and its duration to avoid thermal fatigue in the reactor components, Table 1. To this end, we focused on local compensation schemes for SRF faulty-cavities that allow us a fast beam operation recovery [13,14]. The general strategy for fast compensation of an SRF faulty-cavity are the following:

- Abnormal cavity behavior is detected.
- Fast faulty-cavity detuning.
- Beam operation is stopped.
- The compensation settings are uploaded.
- The beam operation is resumed.

The entire process must take few seconds to fulfill the reliability requirements.

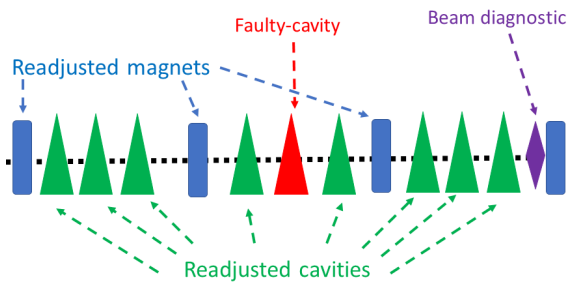


Figure 5: SRF cavity compensation scheme. The setting of the non faulty-cavities and the magnets were re-adjusted to recovery similar conditions as the baseline operation.

Figure 5 illustrates the SRF cavity compensation scheme. The settings of the cavities that surround the faulty-cavity are re-adjusted. The $E_{acc}$ of the compensated cavities increased up to 20 % of its operational value. This constraint reduces potential risks to operate with high electromagnetic fields inside the SRF structure. The synchronous phase ($\phi_s$) was allowed to change ±50 % around its baseline value to avoid a large reduction of the phase acceptance. In addition, we adjusted the magnets to reduce the mismatch.

Figure 6 presents the compensation scheme for a failure in the last cavity of the EllipR1 section, cavity 223. For this case, the $\phi_s$ and the $E_{acc}$ of the faulty-cavity drooped to zero. The compensation was achieved by re-adjusted the voltage and phase of four upstream cavities of the faulty one and three downstream cavities.

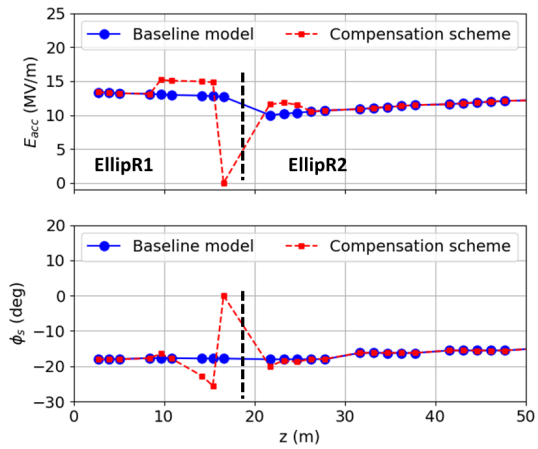


Figure 6: Compensation scheme for the failure in the last EllipR1's cavity. The black-dotted vertical line indicates the transition between EllipR1 and EllipR2 regions.

The increase of $E_{acc}$ and $\phi_s$ did not exceed the limits of 20 % and 50 %, respectively, of their baseline values. A close-up of the beam energy plot near the location where the compensation scheme is applied is shown in Fig. 7. We see that at the beginning of the compensation scheme, the beam energy is increased. Then, at the faulty-cavity location, no energy gain is observed, and finally, in the following three SRF structures downstream, the beam energy reached the performance of the beam design.

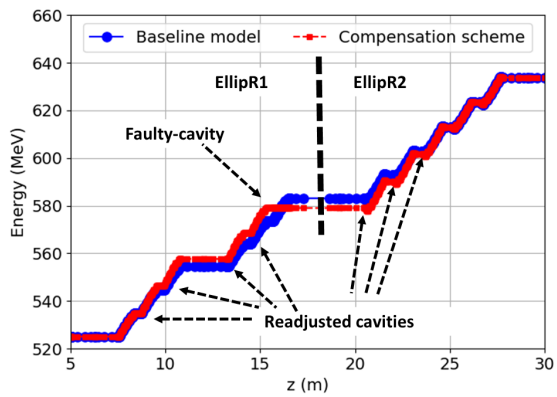


Figure 7: Beam energy for compensation scheme for the failure in the last EllipR1's cavity. The SRF cavity positions are indicated by the black-dotted arrows.

The efficiency of the compensation scheme was tested by computed the emittance, mismatch, and energy concerning the baseline model. To this end, we carried out beam tracking simulations using $2x10^5$ macroparticles. The compensation scheme performance was evaluated first locally by simulated a lattice portion that contains the faulty-cavity and few periods upstream and downstream. This way allowed a fast way to test and select potential schemes. Then, the selected schemes were tracked until the end of the linac, and

ISBN: 978-3-95450-233-2 ISSN: 2673-5504 doi:10.18429/JACoW-SRF2021-TUPFAV001

the beam parameters were compared against the baseline model. Table 5 presents the results of SRF faulty-cavity schemes in crucial sections of the ADS linac. N stands for the number of cavities upstream and downstream of the faulty-cavity.

Table 5: Summary of SRF Faulty-cavity Schemes
The beam parameters are compared to the baseline one at the end of the linac.

| **Faulty cavity** | **293** | **223** | **91** |
|---|---|---|---|
| Description | Last cavity of EllipR2 | Transition between EllipRs | Transition between SSRs |
| $N_{up}$ - $N_{down}$ | 5-0 | 4-3 | 3-3 |
| $\Delta\varepsilon_{norm,rms,t}$ (%) | 0 | 0.6 | -0.1 |
| $\Delta\varepsilon_{norm,rms,z}$ (%) | 0 | 1.8 | 2.9 |
| $\text{Mismatch}_t$ (%) | 0.04 | 0.01 | 0.01 |
| $\text{Mismatch}_z$ (%) | 0.12 | 0.05 | 0.02 |
| $\Delta E$ (%) | 0.02 | 0 | 0 |

In general, lower mismatches and energy differences were obtained in all the SRF sections. However, from the middle to the start of SSR1's section, the emittance difference reached 35%. Moreover, the compensation schemes in the HWR section produced beam losses and large beam degradation. Thus, we decided to implement this scheme only for SSRs and EllipRs regions.

## CONCLUSIONS

The JAEA-ADS linac required a reliability-oriented design. To this end, the linac model is developed to achieve a robust optics design and fault-tolerance capabilities. The main linac has five SRF sections operated with 293 de-rated cavities with a total length of 416 m. The beam optics design has good control of emittance growth and the beam envelopes along the linac that result in the absence of beam loss. The linac model can use fault-tolerance schemes for a fast linac operation recovery in case of cavities failures on the SSRs and EllipRs region, without severe degradation of the final beam parameters and compromise the operation of the superconducting cavities.

## ACKNOWLEDGMENTS

The authors would like to thank to the members of the JAEA-ADS for their comments and suggestions.

## REFERENCES

[1] K. Tsujimoto *et al.*, "Neutronics design for lead-bismuth cooled accelerator-driven system for transmutation of minor actinide", *JNST*, vol. 41, no. 21, p. 21, Jan. 2004. doi:10.1080/18811248.2004.9715454

[2] C. C. Peters, G. D. Johns, S.-H. Kim, and A. P. Shishlo, "Demonstration of Superconducting RF Linac Flexibility for High Power Linacs ", presented at the 11th Int. Particle Accelerator Conf. (IPAC'20), CAEN, FRANCE, May 2020, paper TUVIR16.

[3] H. Takei, private communication, Jun. 2021.

[4] J.L. Biarrotte, "Reliability and fault tolerance in the European ADS project", CERN, Geneva, Switzerland, Rep. CERN-2013-001.481, Jun. 2011.

[5] H. Takei, K. Nishihara, K. Tsujimoto, and H. Oigawa, "Estimation of acceptable beam-trip frequencies of accelerators for accelerator- driven systems and comparison with existing performance data", *J. Nucl. Sci. Techol.*, vol. 49, p. 384, Sep. 2012. doi:10.1088/00223131.2012.669239

[6] J.-F. Ostiguy, J.-P. Carneiro, N. Solyak, and A. Vostrikov, "Overview of beam optics in Project-X superconducting SC CW Linac ", in *Proc. 46th ICFA Advanced Beam Dynamics Workshop on High- Intensity and High-Brightness Hadron Beams (HB'10)*, Morschach, Switzerland, Sep.-Oct. 2010, paper TUO1B04, pp. 314–318.

[7] Z. Li *et al.*, "Physics design of an accelerator for an accelerator-driven subcritical system", *Phys. Rev. ST Accel. Beams*, vol. 16, p. 080101, Dec. 2013. doi:10.1103/PhysRevSTAB.16.080101

[8] D. Vandeplassche, J.-L. Biarrotte, H. Klein, and H. Podlech, "The Myrrha Linear Accelerator", in *Proc. 2nd Int. Particle Accelerator Conf. (IPAC'11)*, San Sebastian, Spain, Sep. 2011, paper WEPS090, pp. 2718–2720.

[9] B. Yee-Rendon, Y. Kondo, F. Maekawa, S. Meigo, and J. Tamura, "Beam optics design of the superconducting region of the JAEA ADS ",*J. Phys. Conf. Ser.*, vol. 1350, p. 12120, Sep. 2019. doi:10.1088/1742-6596/1350/1/012120

[10] B. Yee-Rendon *et al.*, "Present Status of the R&D of the Superconducting Linac for the JAEA- ADS", *J. Phys. Soc. Jpn.*, vol. 33, p. 011043, March 2021. doi:10.7566/JPSCP.33.011043.

[11] TraceWin Manual, http://irfu.cea.fr/dacm/logiciels

[12] Y. Kondo, J. Tamura and B. Yee-Rendon, "Reference Design of the RFQ for JAEA ADS Linac", *JPS Conf. Proc.*, vol. 33, p. 011015, March 2021. doi:10.7566/JPSCP.33.011015.

[13] J.-L. Biarrotte, M. Novati, P. Pierini, H. Safa, and D. Uriot, "Beam Dynamics Studies for the Fault Tolerance Assessment of the PDS-XADS Linac Design",in *Proc. 9th European Particle Accelerator Conf. (EPAC'04)*, Lucerne, Switzerland, Jul. 2004, paper TUPLT057, pp. 1282–1284.

[14] F. Bouly, J.-L. Biarrotte, and D. Uriot, "Fault Tolerance and Consequences in the MYRRHA Superconducting Linac ",in *Proc. 27th Linear Accelerator Conf. (LINAC'14)*, Geneva, Switzerland, Aug.-Sep. 2014, paper MOPP103, pp. 297–299.